FULL-LENGTH PAPER

THE PROTEIN SOCIETY WILEY

The MECP2-TRD domain interacts with the DNMT3A-ADD domain at the H3-tail binding site

Stefan Kunert[1] | Verena Linhard[2] | Sara Weirich[1] | Michel Choudalakis[1] | Florian Osswald[1] | Lisa Krämer[1] | Anja R. Köhler[1] | Alexander Bröhm[1] | Jan Wollenhaupt[3] | Harald Schwalbe[2] | Albert Jeltsch[1]

[1]Institute of Biochemistry and Technical Biochemistry, University of Stuttgart, Stuttgart, Germany

[2]Center for Biomolecular Magnetic Resonance (BMRZ), Institute for Organic Chemistry and Chemical Biology, Goethe University, Frankfurt, Germany

[3]Macromolecular Crystallography Group, Helmholtz-Zentrum Berlin, Berlin, Germany

Correspondence
Albert Jeltsch, Institute of Biochemistry and Technical Biochemistry, University of Stuttgart, Allmandring 31, 70569 Stuttgart, Germany.
Email: albert.jeltsch@ibtb.uni-stuttgart.de

Abstract

The DNMT3A DNA methyltransferase and MECP2 methylation reader are highly expressed in neurons. Both proteins interact via their DNMT3A-ADD and MECP2-TRD domains, and the MECP2 interaction regulates the activity and subnuclear localization of DNMT3A. Here, we mapped the interface of both domains using peptide SPOT array binding, protein pull-down, equilibrium peptide binding assays, and structural analyses. The region D529-D531 on the surface of the ADD domain was identified as interaction point with the TRD domain. This includes important residues of the histone H3 N-terminal tail binding site to the ADD domain, explaining why TRD and H3 binding to the ADD domain is competitive. On the TRD domain, residues 214–228 containing K219 and K223 were found to be essential for the ADD interaction. This part represents a folded patch within the otherwise largely disordered TRD domain. A crystal structure analysis of ADD revealed that the identified H3/TDR lysine binding pocket is occupied by an arginine residue from a crystallographic neighbor in the ADD apoprotein structure. Finally, we show that mutations in the interface of ADD and TRD domains disrupt the cellular interaction of both proteins in NIH3T3 cells. In summary, our data show that the H3 peptide binding cleft of the ADD domain also mediates the interaction with the MECP2-TRD domain suggesting that this binding site may have a broader role also in the interaction of DNMT3A with other proteins leading to complex regulation options by competitive and PTM specific binding.

KEYWORDS
DNA methylation, DNMT3A, MECP2, protein/protein interaction

1 | INTRODUCTION

In mammals, DNA-(cytosine C5)-methylation mostly at CpG sites is involved in the control of gene expression,

regulation of parental imprinting, X chromosome inactivation, and development (Chen & Zhang, 2020; Schubeler, 2015). Furthermore, DNA methylation has an influence on cellular reprogramming, brain function, and behavior (Jang et al., 2017; Kinde et al., 2015). Alterations in the DNA methylation pattern are implicated in cancer, as well as psychiatric diseases and diseases of the immune system (Hamidi et al., 2015; Liu et al., 2018a). The enzymes which are responsible for DNA methylation are called DNA methyltransferases (DNMTs) and they catalyze the methylation reaction of transferring an activated methyl group from the S-adenosyl-L-methionine (AdoMet) cofactor to the C5 position of the pyrimidine ring of a cytosine base (Jeltsch, 2002). Cytosines in the mammalian genome are mainly methylated at palindromic CpG sites on both DNA strands (Jeltsch et al., 2019a; Schubeler, 2015). CpG sites within CpG-rich sequences, so-called CpG islands, which occur in promotor regions of many human genes, are usually not methylated. Beside CpG methylation, DNA-(cytosine C5)-methylation also occurs at non-CpG sites (CpA, CpT, and CpC), in mammals especially in embryonic stem cells and neurons (He & Ecker, 2015). Non-CpG methylation is introduced by the DNMT3A (Dukatz et al., 2022) and DNMT3B (Dukatz et al., 2020) DNA methyltransferases and it plays an important role in brain development, though the function of non-CpG methylated sites is not yet fully understood (Guo et al., 2014; Kinde et al., 2015). DNA methylation functions as a regulator of chromatin structure and gene expression by controlling the recruitment of transcription factors (Kribelbauer et al., 2017; Maurano et al., 2015; Yin et al., 2017) and protein complexes containing subunits with a methyl-CpG-binding domain (MBD) (Liu et al., 2018b; Shimbo & Wade, 2016). The DNA methylation pattern of the genome is generated and maintained in a dynamic process with cytosines being continuously methylated and demethylated (Jeltsch & Jurkowska, 2014). The steady-state methylation level at CpG sites is therefore determined by the local activity of DNMTs and demethylases. Reduced levels of DNMT3A in the brain have been shown to lead to behavioral and neurodevelopmental disorders (Christian et al., 2020).

DNMT3A and DNMT3B are so-called de novo DNA methyltransferases, because they methylate DNA without preference for hemimethylated target sites (Gowher & Jeltsch, 2018). They consist of a regulatory N-terminal multidomain part and a catalytic C-terminal domain. The N-terminal part of DNMT3A comprises three chromatin interaction domains, a ubiquitin-dependent recruitment region which binds to H2AK119ub1 (Weinberg et al., 2021), a proline-tryptophan-tryptophan-proline (PWWP) domain which binds to H3K36me2/3 (Baubec et al., 2015; Dhayalan et al., 2010; Jeltsch & Jurkowska, 2016; Weinberg et al., 2019) and an ATRX-DNMT3-DNMT3L (ADD) domain binding to the unmodified N-terminus of the H3-tail (Jeltsch & Jurkowska, 2016; Zhang et al., 2010) (Figure 1a). H3-tail binding of the ADD domain is mediated by the H3 N-terminal amino group and the K4 side chain, which interacts with amino acid residues D529 and D531 of the ADD domain (Figure 1b) (Guo et al., 2015; Otani et al., 2009). Methylation or acetylation of the H3K4 residue disrupt the ADD domain interaction (Otani et al., 2009; Zhang et al., 2010). The ADD domain is involved in allosteric regulation of DNMT3A by binding to the catalytic domain of the enzyme on two distinct interfaces: (1) binding of the ADD domain to a so-called allosteric site keeps the catalytic pocket accessible for DNA allowing DNA methylation. (2) Binding of the ADD domain to an inhibitory site on the catalytic domain blocks the access of the DNA to the catalytic domain and leads to autoinhibition (Guo et al., 2015; Jeltsch & Jurkowska, 2016). The H3-tail interaction stabilizes the ADD domain binding to the allosteric binding site leading to an increase in the catalytic activity of DNMT3A. In addition, the ADD domain functions as a platform for the interaction of DNMT3A with other proteins including the TRD domain of the methyl-CpG-binding protein 2 (MECP2) (Rajavelu et al., 2018).

MBD family proteins (including MBD1, MBD2, MBD3, and MECP2) are involved in the organization of the chromatin and regulation of gene expression (Jeltsch et al., 2019b; Liu et al., 2018b; Shimbo & Wade, 2016). These proteins bind to methylated CpGs via their MBD and act as DNA methylation-mediated transcriptional repressors by recruiting downstream factors which increase chromatin condensation and remove activating chromatin signals. MECP2 is one member of the MBD protein family (Ausio et al., 2014). It binds specifically to a methyl-CpG pair and methylated cytosines in a non-CpG context (Gabel et al., 2015; Kinde et al., 2015; Lei et al., 2019). Beside the MBD domain, MECP2 contains several AT-hook domains, which bind to the DNA next to the CpG site and ensure the high DNA binding affinity (Klose et al., 2005), a nuclear localization signal (NLS) and a transcription repression domain (TRD). However, structure prediction programs indicate that large parts of the MECP2 protein are in a natively unfolded state (Figure 1c) (Ausio et al., 2014). The TRD domain has been shown to function as a recruitment platform for proteins involved in gene repression (Della Ragione et al., 2016), like the mSin3A corepressor complex and histone deacetylases (Nan et al., 1998) or the chromatin remodeling protein ATRX (Kernohan et al., 2014). However, MECP2 was shown to activate gene expression as
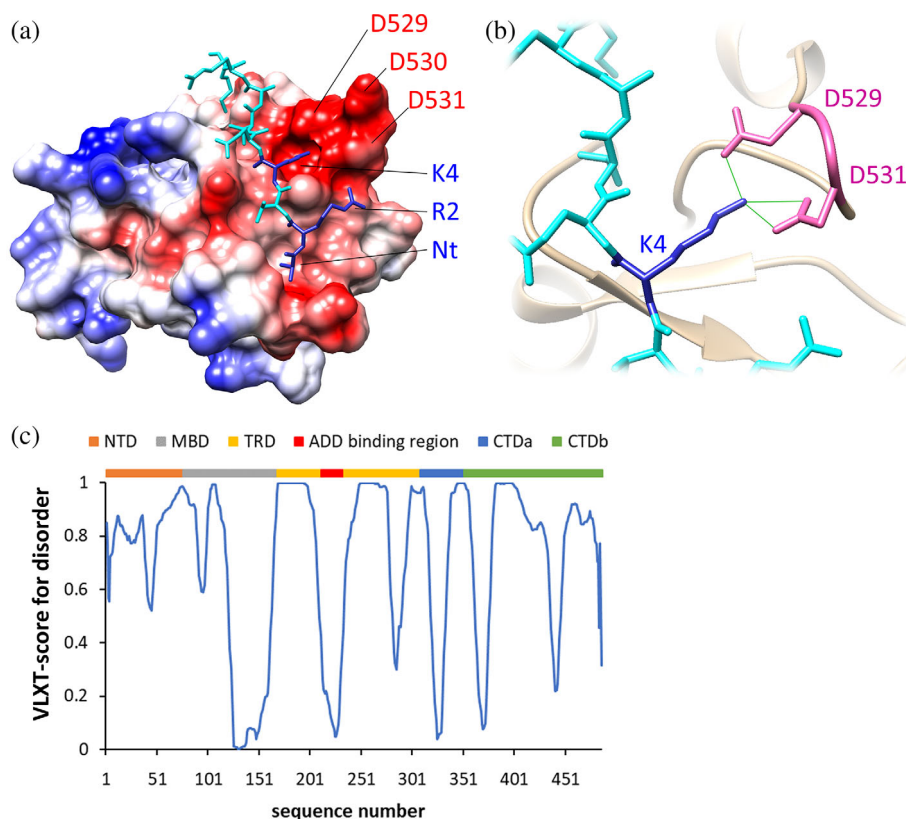
FIGURE 1 Structure of the ADD and TRD domains. (a) Structure of the DNMT3A-ADD domain (PDB 4U7T)(Guo et al., 2014) with bound H3 peptide. The ADD domain is shown in surface representation colored by the coulomb potential from −10 kcal/(e mol) in red to +10 kcal/(e mol) in blue. The D529, D530, and D531 residues (numbering refers to full length DNMT3A) are indicated. The peptide is shown in cyan, with the N-terminus, R2 and K4 indicated and colored in blue. (b) Detail of the interaction of DNMT3A-ADD with the H3K4 residue showing the direct H-bonds formed between K4 and D529 as well D531. (c) Domain structure and disorder prediction of the MECP2 protein. The VLXT score is a measure for the likelihood of intrinsic disorder. It was predicted using the predictor of natural disordered regions sever (http://www.pondr.com/) (Xue et al., 2010). The ADD binding region identified within the TRD domain is indicated in red. NTD, N-terminal domain, MBD, methylcytosine binding domain; TRD, transcriptional repression domain; CTDa, C-terminal domain part a; CTDb, C-terminal domain part b

well by interacting with transcriptional activators like CREB1 (Ben-Shachar et al., 2009; Chahrour et al., 2008). MECP2 is highly expressed in brain tissue and crucial for the maturation and maintenance of neurons (Gulmez Karaca et al., 2019; Tillotson & Bird, 2019). Due to its high expression in neurons, mutations or alterations in the expression level of MECP2 are involved in different neuropathological disorders like autism, Down syndrome, or Alzheimer's disease, and especially in Rett syndrome. Rett syndrome affects 1 of 10,000 female live births and belongs to the group of neurodevelopmental disorders. It is caused by mutations in the _MECP2_ gene (Amir et al., 1999), which is X-linked in mammals and therefore affects males more severely than females. MECP2 mutations are found in 95% of Rett syndrome cases (Ausio et al., 2014).

Both, DNMT3A and MECP2 are highly expressed in neurons (Feng et al., 2005; Guy et al., 2011) and they function as a pair of DNA methylation writer and reader.

Both proteins are targeted to pericentromeric heterochromatin (Bachman et al., 2001; Ge et al., 2004) and in a previous work we observed a strong interaction between the ADD domain of DNMT3A and the TRD domain of MECP2 (Rajavelu et al., 2018). However, further details of this protein/protein interaction are unknown despite the critical role of both proteins in human physiology. It was the major aim of this work to structurally characterize the DNMT3A-MECP2 interaction by mapping the interface regions on the ADD and TRD domain.

2 | RESULTS AND DISCUSSION

2.1 | Mapping of the ADD-TRD interface in the ADD domain

We aimed to map the interaction interface of the DNMT3A-ADD and MECP2-TRD domains using a

strategy involving peptide SPOT array binding, mutagenesis of candidate interface residues and GST-pulldown assays. As structural data were available for the DNMT3A-ADD domain, while large parts of MECP2 are predicted to be intrinsically disordered at least in the absence of protein interactors (Figure 1c), we focused on the ADD domain first. We inspected the ADD domain and noticed six putative interaction regions on different faces of the surface (Figure 2a). We prepared peptide SPOT arrays presenting ADD peptides from these regions and screened them for potential TRD interaction. Variants of the ADD peptides containing double and triple alanine mutants of central amino acids were included in the SPOT arrays as well to control for the specificity of the binding signal. The arrays were incubated with the purified GST-tagged TRD domain (Figure S1a) and resulted in the identification of three peptides, which showed TRD binding with the WT sequence, but displayed a loss of TRD binding upon mutation (ADD 496–510 with 501–503 and 504–506 mutants, ADD 522–536 with 529–531 mutant, and ADD 592–606 with 595–598 mutant) (Figure 2a).

Next, we aimed to investigate ADD-TRD binding at the protein domain level. To this end, ADD was cloned and purified as maltose-binding protein (MBP) fusion (Figure S1b), and a GST-pulldown assay was conducted with GST-TRD to investigate the ADD-TRD interaction. Free GST and MBP domains were used as controls. A strong and specific pulldown was detected, illustrating the stable interaction of both proteins (Figure 2b). To map the TRD interaction on the ADD domain surface, the triple alanine exchange mutations identified in the SPOT array binding experiments were introduced into the ADD domain. The mutated ADD domains were purified (Figure S1b) and used in GST-pulldown assays showing a stable interaction in almost all cases that was only reduced by the D529A/D530A/D531A triple mutation (Mut3 in Figure 2c). Finally, we aimed to investigate the individual role of each of the three residues mutated in the triple mutant and prepared individual D529A, D530A, and D531A single mutants of the MBP-ADD domain, which were purified (Figure S1b) and used in GST-pulldown experiments with GST-TRD (Figure 2d). The data revealed a reduction of the interaction by each of the mutations, presumably because mutation of any of them can affect the conformation of the entire loop. In conclusion, the peptide region D529–D531 on the surface of the ADD domain was identified as an interaction point with the TRD domain. Our data indicate that all three aspartic acid residues are important. Interestingly, this site represents the binding site of the unmethylated K4 of the H3 peptide to the ADD domain (Figure 1a,b) explaining the previous finding that H3-tail binding is competitive with TRD binding to ADD (Rajavelu et al., 2018).

2.2 | Mapping of the ADD-TRD interface in the TRD domain

Lacking structural information for the TRD domain, a hypothesis driven approach was applied to identify the ADD-binding interface. Biochemical data showed that the positively charged N-terminus and K4 of the H3-tail peptide are essential for its ADD interaction (Otani et al., 2009; Zhang et al., 2010). We therefore speculated that clusters of basic residues will also mediate the interaction of TRD with ADD. This conjecture was further supported by the identification of the acidic D529/D530/D531 loop as TRD contact point on the ADD domain. We inspected the TRD sequence and identified all stretches with clustered K and/or R residues (Figure 3a). The candidate peptides were prepared on peptide SPOT arrays and binding was tested with the MBP-ADD domain (Figure 3b). The data revealed a strong interaction with one of the spots comprising the TRD residues 214–228 which contains K219 and K223. Binding was lost with the ADD D529A/D530A/D531A triple mutant indicating that it occurred at the previously identified binding site (Figure 3b). Peptide array binding experiments with TRD 214–228 mutant peptides in which both lysine residues were exchanged by alanine or glutamate showed loss of binding supporting the central role of these lysine residues in the binding interaction (Figure 3c). Next, we tested the role of K219 and K223 for the TRD-ADD domain binding interaction in the pulldown assay using TRD domains containing single or double lysine to alanine mutations at these sites (Figure 3d, Figure S1a). The results indicated that each of the mutations led to a reduced pulldown signal which confirmed that this part of TRD is involved in the ADD interaction. Strikingly, the 214–226 region is located within the largest structured subregion of the otherwise largely disordered TRD domain (Figure 1c).

2.3 | Equilibrium binding experiments of the TRD peptide to the ADD domain

We next aimed to confirm these findings in an equilibrium peptide binding experiment using a purified peptide substrate. To further map and restrict the regions of TRD necessary for ADD binding, peptide SPOT arrays were synthesized containing different parts of the TRD 214–228 region and binding of the ADD domain was tested (Figure 4a). The data revealed a strong reduction of binding to peptides lacking F226. We concluded that this residue is essential for the interaction and purchased a TRD 216–226 peptide as potential minimal binding substrate that is symmetrical on the double-K and contains F226.
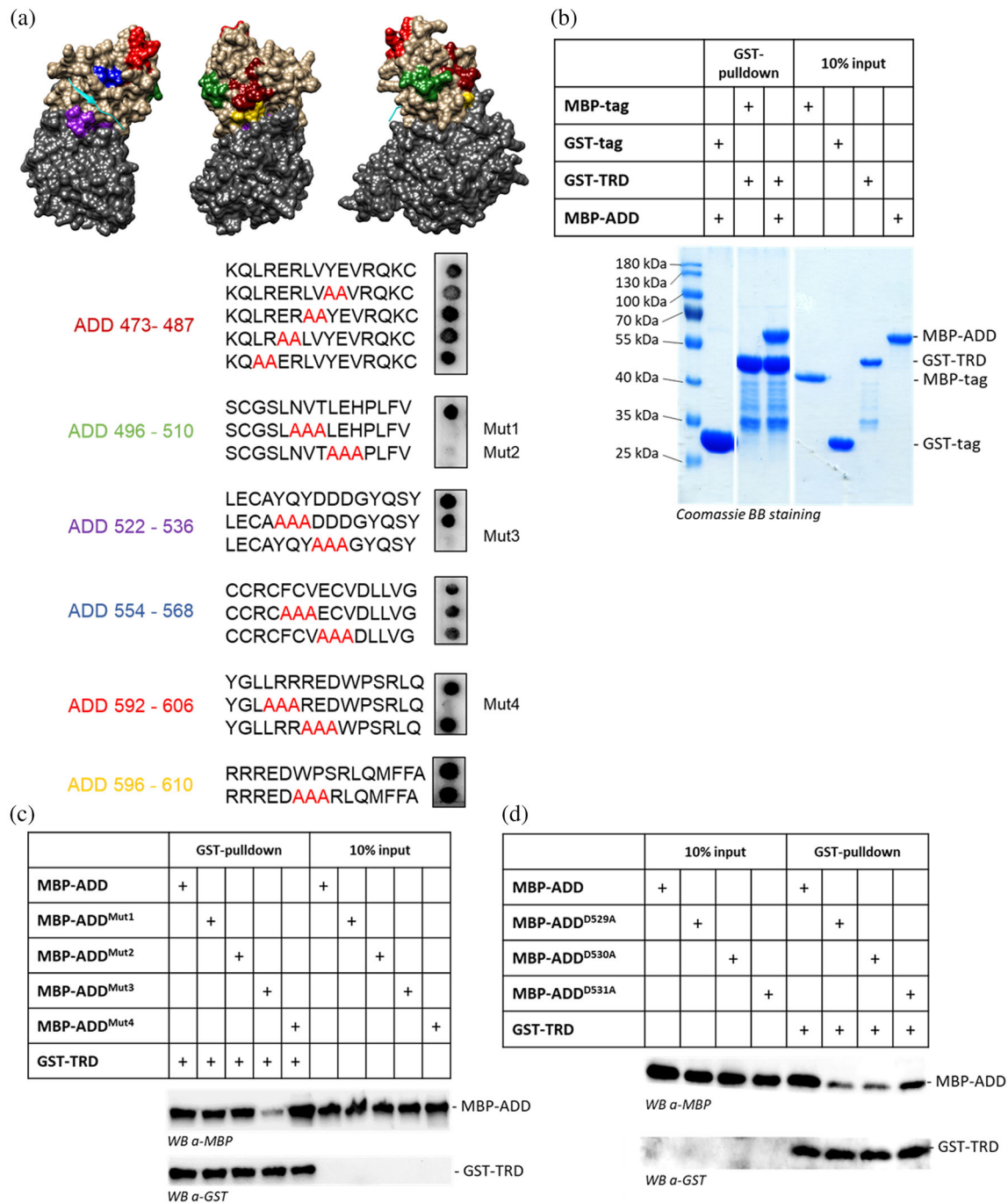
FIGURE 2 Mapping of the DNMT3A-ADD/MECP2-TRD interface in the ADD domain. (a) Binding of the GST-TRD domain to peptide SPOT arrays presenting ADD peptides. The top part of the image shows the structure of a DNMT3A fragment (PDB 4U7T) (Guo et al., 2014) comprising the ADD (brown) and catalytic domain (gray) in three orientations. The H3 peptide is in cyan. The candidate regions for TRD interaction are highlighted. In the lower part, TRD interaction was tested with peptide SPOT arrays containing the corresponding ADD surface peptides and peptides with double or triple mutations of amino acids in the central parts of the sequence. (b) GST-pulldown experiments with GST-TRD and MBP-ADD domains. (c) GST-pulldown experiments with GST-TRD and MBP-ADD WT and complex mutant domains. Mutant 1 N501-T503 to AAA, mutant 2: L504-H506 to AAA, mutant 3: D529-D531 to AAA, mutant 4: L595-R597 to AAA. (d) GST-pulldown experiments with GST-TRD and MBP-ADD WT and single mutant domains

An FITC was included at the N-terminus of the peptide for detection. To exclude any potential effect of the GST-tag on the peptide binding, the GST-ADD protein with cleaved-off GST-tag prepared for the crystallization studies (see below) was used for the equilibrium peptide binding experiments (Figure S1c). ADD binding was detected
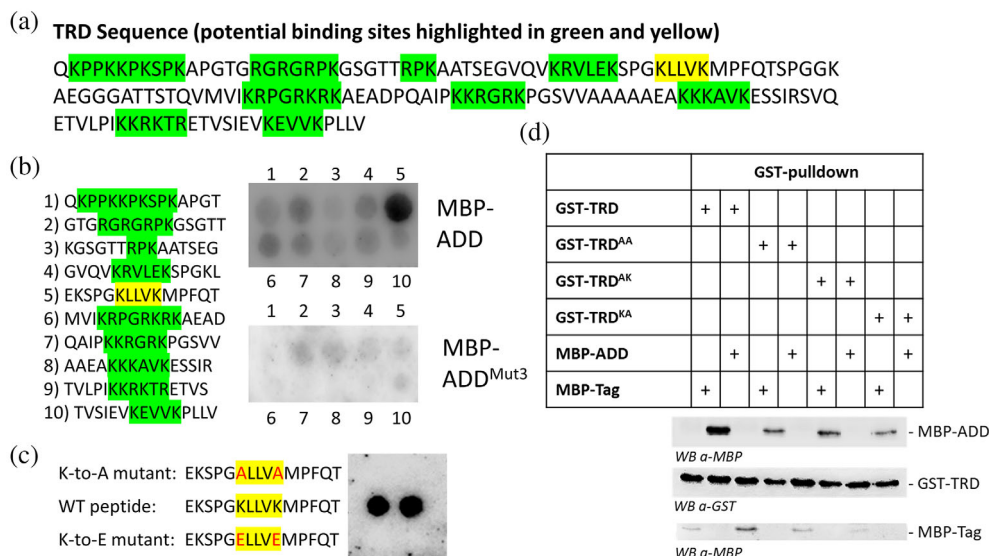
FIGURE 3 Mapping of the DNMT3A-ADD/MECP2-TRD interface in the TRD domain. (a) Compilation of potential K/R rich ADD binding motifs in the primary sequence of the TRD domain labeled in green. The finally identified site is shown in yellow. (b) Peptide SPOT binding experiments of WT GST-ADD WT and mutant 3 (D529-D531 to AAA) to 15mer peptides containing the potential binding sites. (c) Peptide SPOT binding experiments of WT GST-ADD to 15mer peptides containing motif 5 of panel B (TRD residues E214-T228, WT peptide) and mutants of the peptide in which both lysine residues (K219 and K223) are exchanged by A (K-to-A mutant) or E (K-to-E mutant). (d) GST-pulldown experiments with the MBP-ADD domain and GST-TRD WT and K219A (AK), K223A (KA) and K119A/K223A (AA) mutants
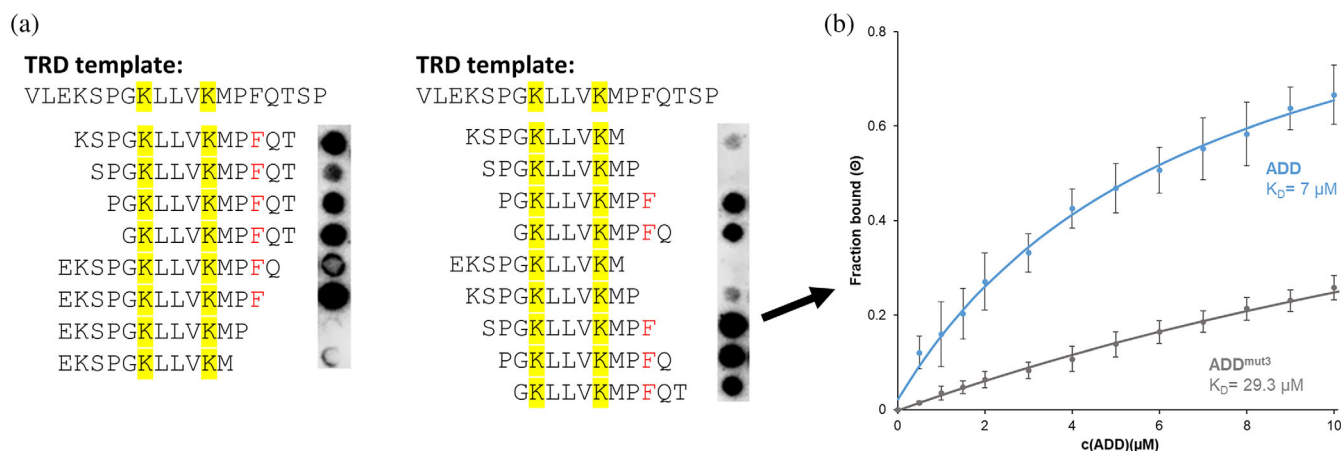

FIGURE 4 Equilibrium binding of the TRD peptide to the ADD domain. (a) TRD-ADD binding to peptide SPOT arrays presenting different parts of the TRD binding region showing that removal of F226 led to a strong reduction in binding. (b) Equilibrium binding experiments of ADD and ADD mutant 3 (D299-D213 to AAA) to the purified TRD 216–226 (SPGKLLVKMPF) peptide. Binding was determined by the change in fluorescence polarization using an N-terminal FITC label on the peptide. Binding constants were derived from two independent titration experiments. Error bars show the maximal error of the individual data points

by fluorescence polarization (FP) upon titration of the peptide with increasing concentrations of the ADD domain. We observed a robust peptide binding of the ADD domain with a K_D-value of 7.0 μM (Figure 4b). We have observed competitive binding of the ADD domain to the TRD domain and histone H3 (Rajavelu et al., 2018), and now also observed competitive binding of the TRD and H3 peptides to the ADD domain (Figure S2) indicating that both peptides share their binding site on the ADD domain.

Next, we tested TRD peptide binding by the ADD D529–D531 mutant, which revealed a 4-fold reduced binding constant ($K_D = 29.3$ μM) when compared to WT ADD. However, the maximal FP signal at saturating
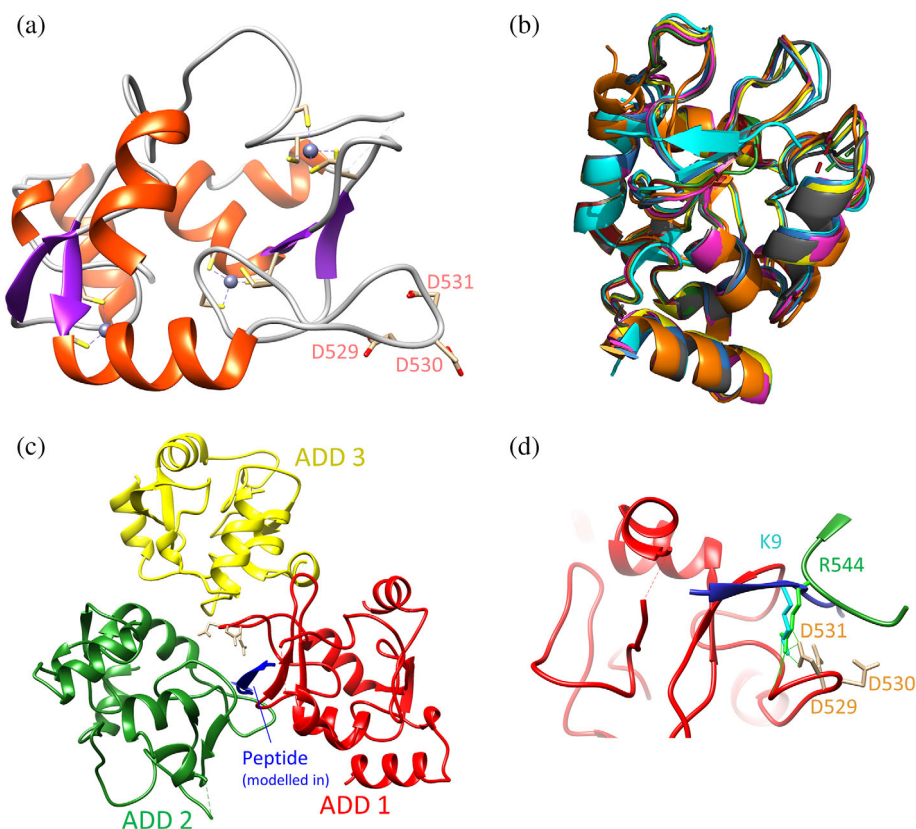
FIGURE 5 Structure of the ADD domain. (a) Ribbon representation of the ADD domain apoprotein structure (colored by secondary structure) with Zn-ions shown as gray spheres. Zn-ion coordinating Cys residues and the D529-D530-D531 residues important for TRD interaction are indicated. (b) Superposition of the structure solved here (green) with available structures of the human DNMT3A ADD domain: ADD 3A1A (red), ADD-H3 complex single chain construct 3A1B (blue), ADD-H3 complex 4QBQ (magenta), ADD G550D-H3 complex 4QBR (yellow), ADD E545R-H3T3ph complex 4QBS (cyan), ADD as part of DNMT3A-DNMT3L 4U7P (orange), ADD as part of DNMT3A-DNMT3L with bound H3 peptide 4U7T (gray). (c) Crystal packing influence in the ADD structure. One ADD subunit is shown as red ribbon with D529, D530 and D531 in tan, and crystallographic neighbors depicted in dark green or yellow ribbon. The ADD-H3 peptide complex (PBD 3A1B) (Otani et al., 2009) was overlayed with the red ADD subunit, only the peptide is shown (blue ribbon). Note that one loop of the green subunit occupies the peptide binding site of the red ADD subunit. Thus, peptide binding would not be compatible with this crystal packing. (d) Detail of the ADD structure with coloring as in panel C showing the red subunit with D529, D530, and D531 as stick representation in orange, the modeled peptide in blue ribbon with K9 as stick representation in cyan and the C541-V546 loop of the green subunit with R544 as stick representation in light green. H-bonds of R546 to the side chain of D531 and backbone carbonyl oxygens of Y533 and Q534 are indicated. Note that R544 occupies the same position as K9 in the H3 complex structure

concentrations of ADD derived in the fitting of the mutant binding curves was considerably higher (3.5-fold) than the maximal FP signal observed with the WT ADD domain. This observation indicates that the peptide binds to the WT and mutant domains in different conformations and in the mutant ADD-peptide complex the FITC probe is more restricted in its movement. This finding suggests that peptide binding to the mutant domain occurs at another binding site and it may include a direct interaction of the FITC group with a binding pocket in the ADD domain. In contrast, in the H3-tail like binding mode expected for the WT ADD domain, the FITC will be placed at the end of the binding cleft not likely to form interactions with the ADD domain. Hence its mobility is expected to be larger. We conclude that the residual

binding of the peptide to the mutant ADD domain presumably occurs at a different binding site, indicating that the loss of peptide binding at the primary binding site of the mutant ADD domain was even larger than suggested from the comparison of the K_D values. In summary, we identified a protein region of the TRD domain including K219 and K223 that is important for the interaction of TRD with the ADD domain at the D529–D531 surface patch.

2.4 | Structural analysis of ADD

The GST-tagged DNMT3A ADD domain was purified after cleaving off the GST-tag (Figure S1c) and used for

crystallization. The obtained crystals diffracted to 1.45 Å resolution (Table S1) and belonged to space group $P6_122$. The structure was solved by molecular replacement using an existing ADD domain apoprotein structure (PDB entry 3A1A) as a search model. Crystals contained one monomer of ADD per asymmetric unit. The ADD structure (Figure 5a) comprises two zinc fingers, one of the GATA binding protein 1 (GATA1) type and one plant homeodomain (PHD)-type coordinating three Zn atoms (Otani et al., 2009). Amino acids 577–578 are not shown since they did not display a clear electron density, due to high flexibility in this loop region. Comparison of the determined structure (shown in green in Figure 5b) with other human ADD domain structures deposited in the PDB with resolutions between 1.8 and 3.8 Å revealed a very high overall similarity of the structures with root-mean-square deviation for all backbone Cα atoms ranging from 0.19 to 0.83 Å (Figure 5b). Unfortunately, despite several attempts it was not possible to obtain co-crystals of ADD with different versions of the TRD peptide. To rationalize this outcome, we inspected the crystal interactions of the ADD domain and observed that one loop of a crystallographic neighboring subunit (C541–V546) partially occupies the binding pocket of the H3 peptide and by this also the potential binding place of the TRD peptide (Figure 5c). Strikingly, R544 from this loop binds to the same place as K9 of the H3 peptide, where it forms H-

bonds to the side chain of D531 and the backbone of Y533 and Q534 (Figure 5d). We conclude that in the observed packing of the ADD apoprotein in space group $P6_122$, peptide binding is blocked. Indeed, the two known ADD domain structures with bound H3 peptide crystallized in different space groups (3A1B is in $P4_12_12$ and 4QBQ is in $P12_11$), while a lower resolution peptide free structure (3A1A) also crystalized in $P6_122$. We conclude that the crystal packing in our ADD domain apoprotein structure is incompatible with incorporation of the TRD peptide which explains the failure of peptide soaking experiments. At the same time the complex apparently did not possess a favorable interface for creating a different packing, thus in the co-crystallization experiments the peptide free form was still preferred. The contact of R544 from a crystallographic neighbor into the peptide binding cleft emphasizes the central role of basic residues in the binding process, which is in agreement with our observation of the important roles of K219 and K223 of the TRD peptide.

2.5 | Subnuclear localization of the ADD domain and MECP2 in NIH3T3 cells

MECP2 is known to accumulate in the pericentromeric heterochromatin in DAPI-dense foci in the nuclei of
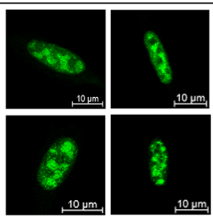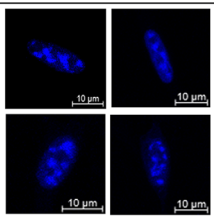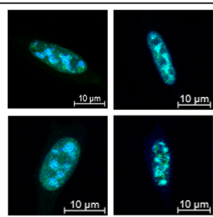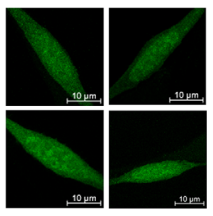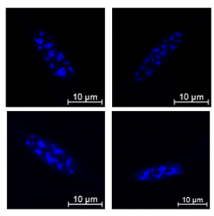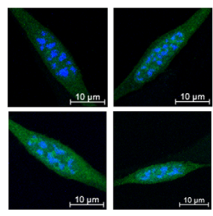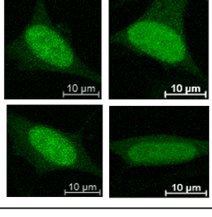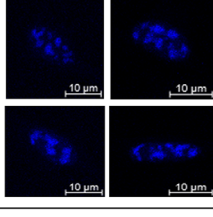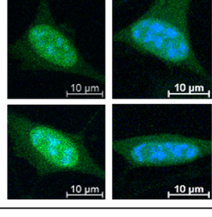
	mVenus channel	eCFP channel	merge	comment
mVenus-ADD + eCFP-MECP2 WT				$N=24$ No other phenotype
mVenus-ADD^{mut3} + eCFP-MECP2 WT				$N=42$ No other phenotype ($p=8.3\times10^{-40}$)
mVenus-ADD + eCFP-MECP2^{KK}				$N=27$ 20 cells show diffuse localization of ADD ($p=9.5\times10^{-14}$)

FIGURE 6 Subnuclear localization of mVenus-ADD and eCFP-MECP2. Experiments were conducted in NIH3T3 cells. The numbers of analyzed cells are indicated. *p*-Values refer to the difference of the mVenus-tagged ADD domain localization between the WT ADD/WT MECP2 sample and the other samples. They are based on a two-sided T-test assuming equal variance. Additional cell images including bright field panels are shown in Figure S4

mouse fibroblasts (Bachman et al., 2001; Ebert et al., 2013; Nan et al., 1996). The same subnuclear localization has been observed with DNMT3A (Bachman et al., 2001; Ge et al., 2004; Jurkowska et al., 2011; Rajavelu et al., 2012). This natural co-localization of both proteins does not allow for direct studies of the effect of MECP2 on the sub-nuclear localization of DNMT3A and vice versa. However, the isolated fluorescently tagged DNMT3A-ADD domain has been shown to have a diffuse nuclear localization that changes to a heterochromatic enrichment after co-expression with MECP2, indicating that MECP2-binding mediates targeting of the ADD domain to heterochromatin (Rajavelu et al., 2018). Based on these previous findings, we have investigated if the binding interface mutations in the ADD and TRD domain identified in this work affect the targeting of the ADD domain to heterochromatin. The mVenus-ADD and eCFP-MECP2 proteins were expressed separately and together in NIH3T3 cells and the spotty, heterochromatic localization of MECP2 as well as the homogenous distribution of ADD were confirmed (Figures 6, S3a, and S4). Co-expression of both proteins led to a redistribution of ADD to heterochromatic foci, which was lost completely for the ADD domain containing the D529A/D530A/D531A mutations (Figures 6 and S4). Interestingly, in single transfections, the introduction of the D529A/D530A/D531A triple mutation led to a more diffuse cytoplasmic localization of mVenus-ADD with a reduction of the nuclear fraction when compared with the WT ADD domain (Figure S3b). This result can be explained, because the D529A/D530A/D531A triple mutation disrupts the interaction of the ADD domain with the H3-tail. Hence, it is expected to reduce the sub-nuclear anchorage of ADD, leading to an increase in cytoplasmic localization. Similarly, co-expression of the ADD domain with MECP2 containing the K219A/K223A double mutation resulted in a significant reduction of the recruitment of ADD to heterochromatic foci (Figure 6), although the mutated MECP2 still localized to these regions (Figure S3c). We conclude that the mutations in the interface of ADD and TRD identified in our work disrupt the cellular interaction of both proteins and this leads to a loss of the mutual targeting of the protein to heterochromatic regions in NIH3T3 cells.

3 | CONCLUSIONS

DNMT3A and MECP2 are important proteins in neurons, involved in setting and reading of DNA methylation (Christian et al., 2020; Kinde et al., 2015). We have shown previously that both proteins interact via their ADD and TRD domains. This interaction was shown to contribute to the mutual co-localization of both proteins

at pericentromeric heterochromatin. Moreover, the interaction with MECP2 was shown to have two effects on DNMT3A activity: On the one hand, TRD domain binding has an inhibitory effect on the activity of DNMT3A via an allosteric mechanism by stabilizing the autoinhibitory conformation of DNMT3A. On the other hand, MECP2 could target DNMT3A to DNA regions already containing methylation. Since TRD and H3-tail binding to the ADD domain is competitive at the peptide (Figure S2) and protein level (Rajavelu et al., 2018), H3-tail binding to the DNMT3A-ADD domain at these sites could disrupt the ADD-TRD interaction and release DNMT3A in an active form leading to DNA methylation at MECP2 target regions. Therefore, the interaction of DNMT3A and MECP2 globally inhibits DNMT3A activity, but MECP2 can act also as a recruiter of DNMT3A and establish a positive feedback loop to ensure stable maintenance of heterochromatic DNA methylation.

So far, the interface regions of both domains and further details of interaction were unknown. Here we identify one surface loop of ADD (D529–D531) as essential for TRD binding as well as two lysine residues in TRD (K219 and K223) as the anchor points of ADD binding. Our data suggest that a TRD surface loop containing these lysine residues binds to ADD at the binding site of H3-tail peptide and the two lysine residues of TRD replace the essential N-terminal and K4 amino groups of the H3 peptide. The new information about binding disrupting mutations in ADD and TRD provided here will pave the way for future mechanistic studies investigating the role of the ADD-TRD interaction in cellular model systems. Interestingly, the target region in TRD has been reported to be modified by different posttranslational modifications (PTMs) in Phosphosite Plus (www.phosphosite.org/) (Hornbeck et al., 2015). K219 can be acetylated and K223 sumoylated, which both likely will disrupt the DNMT3A binding, as well as the reported phosphorylation of S216. These data suggest that the interaction of DNMT3A and MECP2 can be dynamically regulated in cells by PTMs at least on the side of MECP2. Moreover, other proteins may interact with the ADD domain using a similar mechanism which would provide additional options for complex regulation processes by mutual competition of ADD binding proteins and the H3-tail.

4 | MATERIALS AND METHODS

4.1 | Protein expression and purification

The ADD domain of DNMT3A (476–614 of Q9Y6K1) and TRD domain of MECP2 (170–325 of NP_004983) were cloned into pGEX-6P2 and pMAL-p2X as N-terminal

GST or MBP fusion proteins. Site directed mutagenesis was conducted by rolling circle PCR and validated by full sequencing of the obtained plasmids. For overexpression, a single colony was used to inoculate a 25 ml LB medium preculture with appropriate antibiotics. After incubation of the preculture at 37°C for 7 h, 5 ml of the preculture were added to a main culture containing 500 ml LB-Medium, appropriate antibiotics and 50 μM $ZnSO_4$ (ADD domains) or trace metals (50 μM $FeCl_3$, 20 μM $CaCl_2$, 10 μM $MnCl_2$, 10 μM $ZnSO_4$, 2 μM $CoCl_2$, 2 μM $CuCl_2$, 2 μM $NiCl_2$, 2 μM Na_2MoO_4,·2 μM Na_2SeO_3, 2 μM H_3BO_3) (TRD domains). Following incubation at 37°C till an $OD^{600\ nm}$ of 0.6–0.8, the main cultures were shifted to 20°C for ADD and 18°C for TRD proteins, IPTG (final concentration 50 mM) was added and the main cultures were incubated for 12–14 h. The cells were harvested with a Sorvall Lynx 4000 centrifuge (Thermo Scientific) at 4°C and 5000 g for 30 min. The cell pellets were resuspended in 30 ml STE-buffer (10 mM NaCl, 1 mM Tris/HCl pH 8.0, 10 μM EDTA) for washing and centrifuged (ROTIXA 50 RS, Hettich) at 5000g for 30 min. The cell pellets were resuspended in 30 ml sonication buffer (GST: 20 mM HEPES pH 8.0, 500 mM KCl 0.2 mM DTT 1 mM EDTA, 10% v/v glycerol; MBP: 30 mM KPi pH 7.0, 500 mM KCl, 0.2 mM DTT, 1 mM EDTA, 10% v/v glycerol) and lysed on ice by sonication (SONOPLUS ultrasonic homogenizer, BANDELIN electronic GmbH & Co. KG, power settings: 20 cycles for 15 s, 20 s pause, Amp 30%). Next, the lysed cells were centrifuged at 40,000g for 1 h (Sorvall LYNX 6000 Superspeed Centrifuge, Thermo Fisher Scientific, Inc.). In the meantime, the column was prepared by putting 700 μl beads (GST: Glutathione Agarose 4B, Machery-Nagel; MBP: Amylose Resin beads, NEB) on the column and equilibration with 30 ml sonication buffer. The supernatant was loaded on the column and washed with 250 ml sonication buffer. For the elution, 2 ml of elution buffer (GST: sonication buffer supplemented with 40 mM Glutathione; MBP: sonication buffer supplemented with 20 mM maltose monohydrate) was added onto the column and the protein was collected in 4–8 fractions. The fractions with the highest concentration were pooled, transferred in a dialysis bag (MWCO 12–14 kDa, Spectra/Por) and dialyzed against dialysis buffer (20 mM HEPES pH 7.0, 200 mM KCl, 0.2 mM DTT, 1 mM EDTA, 10% v/v glycerol) for 2–2.5 h. The concentrations of the proteins were determined by UV spectrophotometry and later confirmed by densitometric analysis of Coomassie stained SDS–polyacrylamide gels. The proteins were aliquoted, frozen in liquid nitrogen and stored at −80°C.

For crystallization, GST-ADD was overexpressed in 10 L LB-Medium as described above. After lysis, the protein was bound to glutathione agarose 4B beads and washed with 150 ml sonication buffer. Subsequently,

2 ml sonication buffer and 60 μl Prescission protease (Cytiva) were added to the beads and incubated overnight at 4°C on a rotary incubator. ADD was washed from the beads with sonication buffer, purified by size exclusion (10 mM Tris/HCl pH 8, 150 mM NaCl, 2 mM DTT) using a Superdex 200 16/600 PG column (GE Healthcare) operated in an NGC Quest 10 Plus System (BioRad). The sample were concentrated to 10 mg/mL with spin filters (MWCO 10 kDa, Merck Millipore). For storage, the samples were aliquoted, snap frozen in liquid nitrogen and stored at −80°C.

4.2 | Peptide SPOT array binding

Peptide SPOT arrays were prepared as described (Bock et al., 2011; Frank, 2002) using cellulose membrane as solid support for peptide synthesis using a MultiPep Rsi Peptide Synthesizer (Intavis Bioanalytical Instruments). Binding assays were conducted basically as described (Bock et al., 2011; Kungulovski et al., 2015). The membranes were incubated in 5% milk solution overnight, then washed three times for 5 min in 1× Phosphate buffered saline with Tween-20 (PBST) (14 mM NaCl, 0.27 mM KCl, 0.43 mM Na_2HPO_4, 0.14 mM KH_2PO_4, 0.005% Tween-20). Afterwards, the membranes were incubated for 5 min in 10 ml interaction buffer (100 mM KCl, 20 mM HEPES pH 7.5, 1 mM EDTA, 10% Glycerol, 0.2 mM DTT). Twenty-five nanomolar of the corresponding interacting proteins was mixed with 10 ml incubation buffer, applied to the membranes and incubated for 1 h. Subsequently, the membranes were washed with 1× PBST and the first antibody was added (Anti-GST, 1:12,000, GE Healthcare; Anti-MBP, 1:10,000, NEB) in 4 ml 1× PBST and 1 ml milk solution. After incubating the mixture for 1 h, the membranes were washed three times for 5 min in 1× PBST. To detect the bound primary antibody, a secondary antibody fused with horseradish peroxidase (HPR) (Anti-goat HRP 1:12,000, GE healthcare; Anti-mouse HRP 1:5,000, Amersham) was added to the membranes (in 4 ml 1x PBST, 1 ml milk solution) and incubated for 1 h. The detection of the binding signals was performed with the ECL detection kit (Thermo Scientific) and the gel documentation system (Fusion SL3500.WL, Peqlab).

4.3 | GST-pulldown experiments

For the GST-pull-down protein interaction assay, 10 μl of Protino® Glutathione Agarose 4B protein binding beads were equilibrated by washing them with 150 μl of the pull-down interaction buffer (25 mM Tris/HCl pH 8, 200 mM KCl, 5 mM $MgCl_2$, 10% v/v glycerol, 0.1% v/v

NP-40, 200 μM PMSF) followed by centrifugation at 4°C and 2000 g for 2 min for three times. The supernatant was discarded and 200 μl interaction buffer was transferred to the GST beads in low-binding tubes. 1 μg of the GST-tagged protein was added and incubated for 1 h at 6°C and constant rotation. After the incubation, the centrifugation step was repeated. The supernatant was discarded, and the beads were washed three times with 200 μl pull-down interaction buffer (25 mM Tris/HCl pH 8, 200 mM KCl, 5 mM MgCl₂, 10% v/v glycerol, 0.1% NP-40, 200 μM PMSF) to resolve unspecific protein binding to the beads. Subsequently, 150 μl pull-down interaction buffer and 1 μg of the other MBP-tagged protein partner were added to the beads, followed by 1 h incubation at 6°C with constant rotation. Afterwards, the washing of the beads was repeated three times followed by the elution of the bound proteins from the beads. To this end, the protein binding beads were mixed directly with 25 μl 2xLAP and incubated for 10 min at 95°C followed by the analysis of the liquid samples by 12% SDS-PAGE.

4.4 | Equilibrium peptide binding experiments

The FITC-SPGKLLVKMPF-CONH2 TRD peptide was purchased at Synpeptide (Shanghai, China). Peptide purity was 96.88% analyzed by HPLC on a Shimadzu Inertsil ODS-SP (4.6 mm × 250 mm × 5 μm) column run in 0.1% TFA using an acetonitrile gradient (20% ACN to 80% ACN, in 25 min). The H3.1 (1–19) peptide was purchased from Intavis AG in HPLC purified form (purity >99%). ADD-peptide binding was analyzed by the change in fluorescence polarization (FP) upon titration of the peptide with ADD using a Jasco FP-8300 spectrofluorometer with an automatic polarizer (FDP-837) basically as described (Pinter et al., 2021). Acquisitions were performed at 23°C, with excitation at 495 nm and emission measured at 520 nm. Slit width was set to 5 nm for both. Two hundred nanomolar of peptide were dissolved in 0.2 ml of binding buffer (20 mM HEPES pH 7.5, 100 mM KCl, 10% v/v glycerol). After cleaving off the GST-tag, the ADD (or ADD D529A/D530A/D531A) proteins were diluted in buffer (20 mM Hepes pH 7, 200 mM KCl, 0.2 mM DTT, 1 mM EDTA, 10% v/v glycerol) and added in aliquots stepwise. Titrations were conducted in at least two technical replicates. For determination of the K_D-values, the data were fitted to a simple binding equilibrium (Equation 1):

$$\text{Signal} = \text{BL} + F * c_{\text{ADD}}/(c_{\text{ADD}} + K_D) \qquad (1)$$

with: K_D = equilibrium dissociation constant, F = signal factor, and BL = baseline.

4.5 | Subnuclear localization studies

Subnuclear localization studies of mVenus-ADD and eCFP-MECP2 proteins were conducted in NIH3T3 cells basically as described (Dukatz et al., 2019; Rajavelu et al., 2018). The cells were seeded on glass slides and transfected with plasmids expressing mVenus-ADD and eCFP-MECP2 using Fugene HD (Promega) according to the manufacturer's instructions. After 48 h, the cells were fixed with 4% paraformaldehyde, mounted in Fluoromount-G solution and examined with a LSM710 confocal microscope (Zeiss) using a Plan-Apochromat 63×/1.4 Oil DIC M27 objective. The laser excitation wavelength was 514 nm for mVenus, 458 nm for eCFP and the emission collection windows were 520–620 nm for mVenus, 463–519 nm for eCFP. After the setting of the lowest and highest stack, Z-stacks were collected with an interval of 0.5 μm. The stacks were superimposed to gain the maximum intensity projection using the lite ZEN 3.0 SR (black edition) and ZEN 3.4 (blue edition) software. For analysis, individual cells were manually assigned to have either a spotty, heterochromatic or a non-spotty, more homogenous nuclear localization pattern in a blinded manner.

4.6 | Protein crystallization, data collection, data processing, and refinement

Crystals of DNMT3A ADD domain (10.6 mg/ml in 10 mM Tris–HCl pH 8.0, 150 mM NaCl, 2 mM DTT) were grown as a vapor diffusion hanging drop experiment using Crystalgen SuperClear Plates (Jena Bioscience) for supplying the reservoir solution (17% PEG 8000, 0.1 M Tris–HCl, 0.2 M magnesium sulfate, pH 8.5) and siliconized 22 mm thick circular cover slides (Jena Bioscience) as drop support. Drops were set by mixing 2 μl of protein with 1 μl reservoir solution and incubated at 291.15 K to initialize crystal formation. Crystals were cryoprotected using reservoir solution supplied with 20% ethylene glycol. Diffraction data were collected on beamline BL14.2 (Mueller et al., 2015) of the BESSY II electron-storage ring, Berlin, Germany at 100 K using a monochromatic X-ray beam ($\lambda = 0.9184$ Å) and a PILATUS3 2 M detector. The data were processed using XDSAPP (Sparta et al., 2016). The structure was solved by molecular replacement with Phaser (McCoy, 2007) using the structure of DNMT3A ADD domain with PDB entry 3A1A (Otani et al., 2009) as a search model. The structure was refined by iterative cycles of manual model building in Coot (Emsley et al., 2010) and automated refinement using phenix.refine version v1.19.2–4158 (Afonine et al., 2012). Relevant statistics for data processing and refinement are listed in Table S1.

Figures containing molecular graphics were prepared using PyMOL Molecular Graphics System, Version 2.4.1 (Schrödinger LCC) and Chimera (Pettersen et al., 2004). Root-mean-square deviations between backbone Cα atoms of different structures were calculated using PyMOL version 2.4.1 (Schrödinger LCC). The structure and associated structure-factor amplitudes have been deposited in the PDB as entry 8BA5.

AUTHOR CONTRIBUTIONS

ACKNOWLEDGMENTS

CONFLICTS OF INTEREST

The authors declare no competing interests.

DATA AVAILABILITY STATEMENT

All biochemical data are provided with this paper and its supplemental information. The structure of the ADD domain and associated structure-factor amplitudes have been deposited in the PDB as entry 8BA5.

ORCID

Albert Jeltsch https://orcid.org/0000-0001-6113-9290

REFERENCES

Afonine PV, Grosse-Kunstleve RW, Echols N, Headd JJ, Moriarty NW, Mustyakimov M, et al. Towards automated crystallographic structure refinement with phenix. Refine Acta Crystallogr D Biol Crystallogr. 2012;68(Pt 4):352–67.

Amir RE, Van den Veyver IB, Wan M, Tran CQ, Francke U, Zoghbi HY. Rett syndrome is caused by mutations in x-linked mecp2, encoding methyl-cpg-binding protein 2. Nat Genet. 1999;23(2):185–8.

Ausio J, Martinez de Paz A, Esteller M. Mecp2: the long trip from a chromatin protein to neurological disorders. Trends Mol Med. 2014;20(9):487–98.

Bachman KE, Rountree MR, Baylin SB. Dnmt3a and dnmt3b are transcriptional repressors that exhibit unique localization properties to heterochromatin. J Biol Chem. 2001;276(34):32282–7.

Baubec T, Colombo DF, Wirbelauer C, Schmidt J, Burger L, Krebs AR, et al. Genomic profiling of DNA methyltransferases reveals a role for dnmt3b in genic methylation. Nature. 2015;520(7546):243–7.

Ben-Shachar S, Chahrour M, Thaller C, Shaw CA, Zoghbi HY. Mouse models of mecp2 disorders share gene expression changes in the cerebellum and hypothalamus. Hum Mol Genet. 2009;18(13):2431–42.

Bock I, Kudithipudi S, Tamas R, Kungulovski G, Dhayalan A, Jeltsch A. Application of celluspots peptide arrays for the analysis of the binding specificity of epigenetic reading domains to modified histone tails. BMC Biochem. 2011;12:48.

Chahrour M, Jung SY, Shaw C, Zhou X, Wong ST, Qin J, et al. Mecp2, a key contributor to neurological disease, activates and represses transcription. Science. 2008;320(5880):1224–9.

Chen Z, Zhang Y. Role of mammalian DNA methyltransferases in development. Annu Rev Biochem. 2020;89:135–58.

Christian DL, Wu DY, Martin JR, Moore JR, Liu YR, Clemens AW, et al. Dnmt3a haploinsufficiency results in behavioral deficits and global epigenomic dysregulation shared across neurodevelopmental disorders. Cell Rep. 2020;33(8):108416.

Della Ragione F, Vacca M, Fioriniello S, Pepe G, D'Esposito M. Mecp2, a multi-talented modulator of chromatin architecture. Brief Funct Genomics. 2016;15(6):420–31.

Dhayalan A, Rajavelu A, Rathert P, Tamas R, Jurkowska RZ, Ragozin S, et al. The dnmt3a pwwp domain reads histone 3 lysine 36 trimethylation and guides DNA methylation. J Biol Chem. 2010;285(34):26114–20.

Dukatz M, Holzer K, Choudalakis M, Emperle M, Lungu C, Bashtrykov P, et al. H3k36me2/3 binding and DNA binding of

the DNA methyltransferase dnmt3a pwwp domain both contribute to its chromatin interaction. J Mol Biol. 2019;431(24): 5063–74.

Dukatz M, Adam S, Biswal M, Song J, Bashtrykov P, Jeltsch A. Complex DNA sequence readout mechanisms of the dnmt3b DNA methyltransferase. Nucleic Acids Res. 2020;48(20): 11495–509.

Dukatz M, Dittrich M, Stahl E, Adam S, de Mendoza A, Bashtrykov P, et al. DNA methyltransferase dnmt3a forms interaction networks with the cpg site and flanking sequence elements for efficient methylation. J Biol Chem. 2022;298(10): 102462.

Ebert DH, Gabel HW, Robinson ND, Kastan NR, Hu LS, Cohen S, et al. Activity-dependent phosphorylation of mecp2 threonine 308 regulates interaction with ncor. Nature. 2013;499(7458): 341–5.

Emsley P, Lohkamp B, Scott WG, Cowtan K. Features and development of coot. Acta Crystallogr D Biol Crystallogr. 2010;66(Pt 4): 486–501.

Feng J, Chang H, Li E, Fan G. Dynamic expression of de novo DNA methyltransferases dnmt3a and dnmt3b in the central nervous system. J Neurosci Res. 2005;79(6):734–46.

Frank R. High-density synthetic peptide microarrays: emerging tools for functional genomics and proteomics. Comb Chem High Throughput Screen. 2002;5(6):429–40.

Gabel HW, Kinde B, Stroud H, Gilbert CS, Harmin DA, Kastan NR, et al. Disruption of DNA-methylation-dependent long gene repression in rett syndrome. Nature. 2015;522(7554):89–93.

Ge YZ, Pu MT, Gowher H, Wu HP, Ding JP, Jeltsch A, et al. Chromatin targeting of de novo DNA methyltransferases by the pwwp domain. J Biol Chem. 2004;279(24):25447–54.

Gowher H, Jeltsch A. Mammalian DNA methyltransferases: new discoveries and open questions. Biochem Soc Trans. 2018;46(5): 1191–202.

Gulmez Karaca K, Brito DVC, Oliveira AMM. Mecp2: a critical regulator of chromatin in neurodevelopment and adult brain function. Int J Mol Sci. 2019;20(18):4577.

Guo JU, Su Y, Shin JH, Shin J, Li H, Xie B, et al. Distribution, recognition and regulation of non-cpg methylation in the adult mammalian brain. Nat Neurosci. 2014;17(2):215–22.

Guo X, Wang L, Li J, Ding Z, Xiao J, Yin X, et al. Structural insight into autoinhibition and histone h3-induced activation of dnmt3a. Nature. 2015;517(7536):640–4.

Guy J, Cheval H, Selfridge J, Bird A. The role of mecp2 in the brain. Annu Rev Cell Dev Biol. 2011;27:631–52.

Hamidi T, Singh AK, Chen T. Genetic alterations of DNA methylation machinery in human diseases. Epigenomics. 2015;7(2): 247–65.

He Y, Ecker JR. Non-cg methylation in the human genome. Annu Rev Genomics Hum Genet. 2015;16:55–77.

Hornbeck PV, Zhang B, Murray B, Kornhauser JM, Latham V, Skrzypek E. Phosphositeplus, 2014: mutations, ptms and recalibrations. Nucleic Acids Res. 2015;43(Database issue):D512–20.

Jang HS, Shin WJ, Lee JE, Do JT. Cpg and non-cpg methylation in epigenetic gene regulation and brain function. Genes (Basel). 2017;8(6):148.

Jeltsch A. Beyond Watson and crick: DNA methylation and molecular enzymology of DNA methyltransferases. Chembiochem. 2002;3(4):274–93.

Jeltsch A, Jurkowska RZ. New concepts in DNA methylation. Trends Biochem Sci. 2014;39(7):310–8.

Jeltsch A, Jurkowska RZ. Allosteric control of mammalian DNA methyltransferases - a new regulatory paradigm. Nucleic Acids Res. 2016;44(18):8556–75.

Jeltsch A, Broche J, Bashtrykov P. Molecular processes connecting DNA methylation patterns with DNA methyltransferases and histone modifications in mammalian genomes. Genes (Basel). 2019a;10(5):566.

Jeltsch A, Broche J, Lungu C, Bashtrykov P. Biotechnological applications of mbd domain proteins for DNA methylation analysis. J Mol Biol. 2019b;432(6):1816–1823.

Jurkowska RZ, Rajavelu A, Anspach N, Urbanke C, Jankevicius G, Ragozin S, et al. Oligomerization and binding of the dnmt3a DNA methyltransferase to parallel DNA molecules: heterochromatic localization and role of dnmt3l. J Biol Chem. 2011; 286(27):24200–7.

Kernohan KD, Vernimmen D, Gloor GB, Berube NG. Analysis of neonatal brain lacking atrx or mecp2 reveals changes in nucleosome density, ctcf binding and chromatin looping. Nucleic Acids Res. 2014;42(13):8356–68.

Kinde B, Gabel HW, Gilbert CS, Griffith EC, Greenberg ME. Reading the unique DNA methylation landscape of the brain: non-cpg methylation, hydroxymethylation, and mecp2. Proc Natl Acad Sci U S A. 2015;112(22):6800–6.

Klose RJ, Sarraf SA, Schmiedeberg L, McDermott SM, Stancheva I, Bird AP. DNA binding selectivity of mecp2 due to a requirement for a/t sequences adjacent to methyl-cpg. Mol Cell. 2005; 19(5):667–78.

Kribelbauer JF, Laptenko O, Chen S, Martini GD, Freed-Pastor WA, Prives C, et al. Quantitative analysis of the DNA methylation sensitivity of transcription factor complexes. Cell Rep. 2017;19(11):2383–95.

Kungulovski G, Kycia I, Mauser R, Jeltsch A. Specificity analysis of histone modification-specific antibodies or reading domains on histone peptide arrays. Methods Mol Biol. 2015;1348: 275–84.

Lei M, Tempel W, Chen S, Liu K, Min J. Plasticity at the DNA recognition site of the mecp2 mcg-binding domain. Biochim Biophys Acta Gene Regul Mech. 2019;1862(9):194409.

Liu C, Jiao C, Wang K, Yuan N. DNA methylation and psychiatric disorders. Prog Mol Biol Transl Sci. 2018a;157:175–232.

Liu K, Xu C, Lei M, Yang A, Loppnau P, Hughes TR, et al. Structural basis for the ability of mbd domains to bind methyl-cg and tg sites in DNA. J Biol Chem. 2018b;293(19):7344–54.

Maurano MT, Wang H, John S, Shafer A, Canfield T, Lee K, et al. Role of DNA methylation in modulating transcription factor occupancy. Cell Rep. 2015;12(7):1184–95.

McCoy AJ. Solving structures of protein complexes by molecular replacement with phaser. Acta Crystallogr D Biol Crystallogr. 2007;63(Pt 1):32–41.

Mueller U, Förster R, Hellmig M, Huschmann FU, Kastner A, Malecki P, et al. The macromolecular crystallography beamlines at bessy ii of the helmholtz-zentrum berlin: current status and perspectives. Eur Phys J Plus. 2015;130(7):141.

Nan X, Tate P, Li E, Bird A. DNA methylation specifies chromosomal localization of mecp2. Mol Cell Biol. 1996;16(1):414–21.

Nan X, Ng HH, Johnson CA, Laherty CD, Turner BM, Eisenman RN, et al. Transcriptional repression by the methyl-

cpg-binding protein mecp2 involves a histone deacetylase complex. Nature. 1998;393(6683):386–9.

Otani J, Nankumo T, Arita K, Inamoto S, Ariyoshi M, Shirakawa M. Structural basis for recognition of h3k4 methylation status by the DNA methyltransferase 3a atrx-dnmt3-dnmt3l domain. EMBO Rep. 2009;10(11):1235–41.

Pettersen EF, Goddard TD, Huang CC, Couch GS, Greenblatt DM, Meng EC, et al. Ucsf chimera--a visualization system for exploratory research and analysis. J Comput Chem. 2004;25(13):1605–12. UCSF Chimera?A visualization system for exploratory research and analysis.

Pinter S, Knodel F, Choudalakis M, Schnee P, Kroll C, Fuchs M, et al. A functional lsd1 coregulator screen reveals a novel transcriptional regulatory cascade connecting r-loop homeostasis with epigenetic regulation. Nucleic Acids Res. 2021;49(8):4350–70.

Rajavelu A, Jurkowska RZ, Fritz J, Jeltsch A. Function and disruption of DNA methyltransferase 3a cooperative DNA binding and nucleoprotein filament formation. Nucleic Acids Res. 2012;40(2):569–80.

Rajavelu A, Lungu C, Emperle M, Dukatz M, Brohm A, Broche J, et al. Chromatin-dependent allosteric regulation of dnmt3a activity by mecp2. Nucleic Acids Res. 2018;46(17):9044–56.

Schubeler D. Function and information content of DNA methylation. Nature. 2015;517(7534):321–6.

Shimbo T, Wade PA. Proteins that read DNA methylation. Adv Exp Med Biol. 2016;945:303–20.

Sparta KM, Krug M, Heinemann U, Mueller U, Weiss MS. Xdsapp2.0. J Appl Cryst. 2016;49:1085–92.

Tillotson R, Bird A. The molecular basis of mecp2 function in the brain. J Mol Biol. 2019;432(6):1602–23.

Weinberg DN, Papillon-Cavanagh S, Chen H, Yue Y, Chen X, Rajagopalan KN, et al. The histone mark h3k36me2 recruits dnmt3a and shapes the intergenic DNA methylation landscape. Nature. 2019;573(7773):281–6.

Weinberg DN, Rosenbaum P, Chen X, Barrows D, Horth C, Marunde MR, et al. Two competing mechanisms of dnmt3a recruitment regulate the dynamics of de novo DNA methylation at prc1-targeted cpg islands. Nat Genet. 2021;53(6):794–800.

Xue B, Dunbrack RL, Williams RW, Dunker AK, Uversky VN. Pondr-fit: a meta-predictor of intrinsically disordered amino acids. Biochim Biophys Acta. 2010;1804(4):996–1010.

Yin Y, Morgunova E, Jolma A, Kaasinen E, Sahu B, Khund-Sayeed S, et al. Impact of cytosine methylation on DNA binding specificities of human transcription factors. Science. 2017;356(6337).

Zhang Y, Jurkowska R, Soeroes S, Rajavelu A, Dhayalan A, Bock I, et al. Chromatin methylation activity of dnmt3a and dnmt3a/3l is guided by interaction of the add domain with the histone h3 tail. Nucleic Acids Res. 2010;38(13):4246–53.

SUPPORTING INFORMATION

Additional supporting information can be found online in the Supporting Information section at the end of this article.